ACSNANO
www.acsnano.org

ARTICLE

Enzyme-Powered Three-Dimensional DNA Nanomachine for DNA Walking, Payload Release, and Biosensing

Xiaolong Yang,[†] Yanan Tang,[†] Sean D. Mason,[†] Junbo Chen,[‡] and Feng Li*[,†]

[†]Department of Chemistry, Centre for Biotechnology, Brock University, St. Catharines, Ontario, Canada L2S3A1
[‡]Analytical & Testing Center, Sichuan University, Chengdu, Sichuan 610064, China

Supporting Information

ABSTRACT: **Herein, we report a DNA nanomachine, built from a DNA-functionalized gold nanoparticle (DNA–AuNP), which moves a DNA walker along a three-dimensional (3-D) DNA–AuNP track and executes the task of releasing payloads. The movement of the DNA walker is powered by a nicking endonuclease that cleaves specific DNA substrates on the track. During the movement, each DNA walker cleaves multiple substrates, resulting in the rapid release of payloads (predesigned DNA sequences and their conjugates). The 3-D DNA nanomachine is highly efficient due to the high local effective concentrations of all DNA components that have been co-conjugated on the same AuNP. Moreover, the activity of the 3-D DNA nanomachine can be controlled by introducing a protecting DNA probe that can hybridize to or dehybridize from the DNA walker in a target-specific manner. This property allows us to tailor the DNA nanomachine into a DNA nanosensor that is able to achieve rapid, isothermal, and homogeneous signal amplification for specific nucleic acids in both buffer and a complicated biomatrix.**

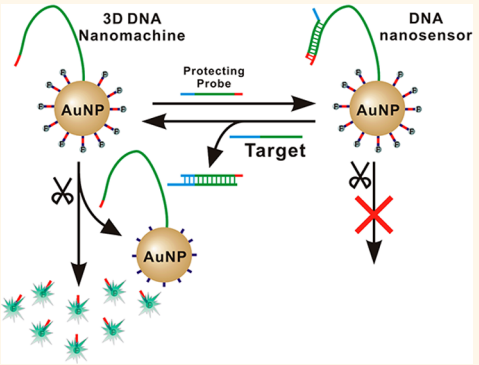

KEYWORDS: *DNA nanotechnology, nanomachine, nicking endonuclease, nanosensors, nucleic acid analysis*

Living systems make use of highly complicated and hierarchical machineries to perform diverse biological functions. Inspired by nature, various artificial molecular machines have also been created.[1−3] A major challenge in engineering molecular machines is to precisely control the mechanical motion of a nanoscale objective along a designated path.[4,5] To meet this challenge, a number of DNA walking devices, including DNA walkers,[5−16] molecular gears,[17] and molecular spiders,[18,19] have been constructed. The success in constructing such devices proves DNA to be versatile and robust building blocks for artificial machineries due to the well-defined Watson–Crick base pairing rule.[5−18] Currently, almost all DNA walking devices make use of one-dimensional (1-D) DNA footpaths[6−12,17,18] or two-dimensional (2-D) DNA origami[13−15,19] as tracks to guide the movement of DNA walkers. Very few well-defined 3-D DNA tracks have been reported so far.[16,20,21] For example, Ellington and co-workers have recently described a stochastic DNA walker that moves randomly on a microparticle surface.[21] Although each walking step is due entirely to autonomous decisions made by the walker, the overall travel space of each DNA walker was well-confined at micrometer space. Construction of such a 3-D DNA walking device demonstrates great potential for applications including biosensing and material assembly. To further expand their functionality, it is desirable to develop 3-D DNA walkers with nanometer precision. Herein, we design a novel DNA nanomachine that is able to confine the movement of a DNA walker on a 3-D track built from DNA-functionalized gold nanoparticles (DNA–AuNPs).

The autonomous movements of DNA machines consume energy. One of the most frequently used energy inputs for DNA walking devices is through the cleavage of DNA substrates along the tracks by endonucleases,[9,10,14,15,20] deoxyribozymes,[11,18,19] or photoirradiation.[12,13] During DNA walking, multiple substrates will be released from the track as a result of the cleavage.[9−15,18−20] While much effort has been emphasized on utilizing DNA walking devices to transport payloads along well-defined tracks and/or to achieve DNA computing,[6−19] there are fewer reports of using such devices for tasks such as targeted payload release or biosensing.[20,21] This is largely due to the relatively slow kinetics and limited moving steps of current devices.[5−19] To this end, we aim to design an integrated 3-D DNA nanomachine that is amenable for tasks including rapid payload release and biosensing.

Received: November 10, 2015
Accepted: January 19, 2016
Published: January 19, 2016

DOI: 10.1021/acsnano.5b07102
ACS Nano 2016, 10, 2324–2330

The principle of our 3-D DNA nanomachine design is illustrated in Scheme 1. The 3-D track is constructed by densely functionalizing a 20 nm diameter gold nanoparticle (AuNP) with DNA substrates (DSs). Single-foot DNA walkers (DWs) are also tethered on the same DNA–AuNP. The DW is designed to have a 7 nt nicking recognition sequence, and the DS is designed to have a 7 nt complementary nicking cleavage sequence. In the presence of the nicking endonuclease, the DW is able to walk along the 3-D track by cleaving one DS at each step. In this design, the direction of each walking step is random, but the overall walking space is well-defined by the 3-D DNA track. To maintain this well-defined walking space, it is critical to minimize the complementary sequences between the DW and the DT to be 7 nt. This is because longer complementary sequences can lead to the "jump" of the DW onto neighboring DNA–AuNP tracks. Longer complementary sequences may also cross-link different nanomachines to form aggregates.

Scheme 1. Schematic Illustrating the Principle of the 3-D DNA Nanomachine Constructed by Co-conjugating DNA Walker and DNA Track (Substrate) Components on a Single AuNP

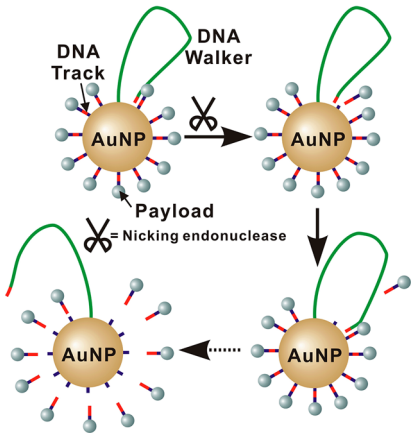

As we aim to achieve the rapid release of payloads, the 3-D DNA nanomachine is designed to carry payloads by conjugating them on DS molecules (Scheme 1). Once DSs are cleaved during DW movement, payloads can be released from the nanomachine. In principle, our design is particularly advantageous to achieve rapid release because the co-conjugation of all DNA components on the same AuNP can greatly increase their local effective concentrations, thus accelerating the enzymatic cleavage. Moreover, our previous success in constructing binding-induced molecular translators[22−25] suggests that the increases in local effective concentrations can also allow sufficient hybridization between the DW and the DS before the cleavage (estimated melting temperature T_m = 51.3 °C, ΔG = −4.49 kcal/mol) and rapid dehybridization after the cleavage (T_m < 0 °C, ΔG = 2.77 kcal/mol).

RESULTS AND DISCUSSION

Construction and Characterization of the 3-D DNA Nanomachine. As a proof-of-principle, we first designed a 3-D DNA nanomachine by attaching a fluorescent dye, FAM, as a payload to the DS. The FAM-labeled DS is then denoted as a signal reporter (SR), and the nanomachine is denoted as DW–SR–AuNP, correspondingly. Initially, FAM on SR was in close proximity with the AuNP, thus the fluorescence was quenched. Once powered by the nicking endonuclease, the DW moves along the 3-D DNA–AuNP track, liberating the FAM-labeled DNA payload, thus turning on the fluorescence (Figure 1a). It has been well-established that nicking endonuclease cleaves only one strand of a double-stranded DNA with high sequence specificity.[26−28] It is essential that this specific enzymatic property is well-maintained when all DNA sequences are co-conjugated on the same AuNP (Figure S1A). To verify the sequence specificity of the nicking endonuclease that has been used to power the 3-D nanomachine, we examined the products from a reaction between 12.5 nM DW–SR–AuNP and 20 U nicking endonucleases using native polyacrylamide gel electrophoresis (PAGE). As shown in Figure S1B, only SR probes are cleaved from the nanomachine, and all DW probes remained intact, verifying the sequence specificity of our 3-D nanomachine design.

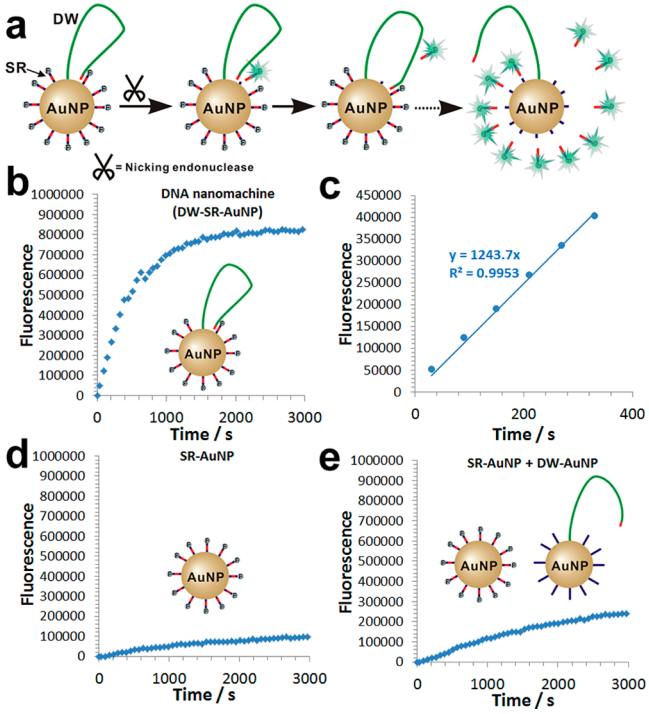

Figure 1. (a) Schematic illustrating the principle of the fluorogenic 3-D DNA nanomachine, DW–SR–AuNP. (b) Monitoring the fluorescence increases as a function of time from 100 pM DW–SR–AuNP. (c) Determining the initial rate of DW–SR–AuNP by monitoring the fluorescence increases every 1 min for the first 5 min. (d) Fluorescence increases as a function of time from a 100 pM SR–AuNP control. (e) Fluorescence increases from the cross-reaction control that consists of 100 pM SR–AuNP and 100 pM DW–AuNP.

To quantitatively characterize the performance of the 3-D DNA nanomachine, we monitored the fluorescence increases in real time using a multimode microplate reader. Figure 1b shows a typical kinetic profile of the DNA nanomachine (DW–SR–AuNP). Immediately after 0.2 U/μL nicking endonuclease was added into a solution containing 100 pM DW–SR–AuNP, a rapid fluorescence increase was observed, which reached saturation within a period of 20 min. The initial rate of the reaction $V_{DW-SR-AuNP}$ was measured to be 5.72 × 10^{-11} M s^{-1}. This rate was determined by measuring the fluorescence

DOI: 10.1021/acsnano.5b07102
ACS Nano 2016, 10, 2324–2330

increase every 1 min for the first 5 min (Figure 1c). To confirm that the rapid fluorescence increase is due to the operation of the DNA nanomachine, we also designed a control DNA–AuNP probe that contained only SR probes (denoted as SR–AuNP). As shown in Figure 1d, a slight fluorescence increase ($V_{SR-AuNP}$ = 3.08 × 10^{-12} M s^{-1}) was observed due to the spontaneous release of SR by the residue dithiothreitol (DTT) associated with nicking endonuclease. This observation confirms that DW is the key component to drive the quick release of FAM-labeled DNA payloads.

To verify that DW moves along the 3-D DNA–AuNP track rather than jumping to cross-react with other nanomachines, we also designed a second control by mixing SR–AuNP with an equal amount of a DW–AuNP control that is conjugated with only the DW probe. To ensure the same DW coverage as for DW–SR–AuNP, DW–AuNP was designed by co-conjugating DW with thiolated poly-dT DNA probes. By comparing the nanomachine with this control (Figure 1e), we found that the rate for DW walking on the correct track (5.72 × 10^{-11} M s^{-1} for DW–SR–AuNP) was 13.5 times faster than that for DW on the incorrect track (4.24 × 10^{-12} M s^{-1} for DW–AuNP control), indicating that more than 90% of DWs are moving on the correct track over a given time period. Collectively, these results suggest that movement of the DW has been well-defined by the 3-D DNA–AuNP track on each nanomachine.

Kinetic Study of the 3-D DNA Nanomachine toward Efficient Payload Release. Having constructed the 3-D DNA nanomachine, we aim to optimize the design to meet the goal of efficient payload release. The 3-D DNA nanomachine is a multicomponent system, and thus each component can potentially have a significant influence on its overall efficiency. To better understand these influences, we quantitatively studied the effect of each component on the kinetics of the nanomachine. Specific parameters include densities of DW (n) and SR (m) on each AuNP, a length of DW (l), and concentrations of nanomachines ([AuNP]) and enzyme ([E]).

We set out to study the effect of the DW design first, including its coverage on AuNP (n) and length (l). To elucidate the effect of the DW coverage, we maximized the coverage of SR (~350) on each AuNP and varied the DW coverage n from 0 to 60 per AuNP. Intuitively, increasing the coverage of DW should result in a higher reaction rate and release more fluorescence payloads. Indeed, this is what we observed when varying n from 0 to 20 per AuNP (Figure 2a). When the measured initial rate V *versus* n was plotted in their logarithmic forms, the data points fit a straight line with the slope close to 1, using least-squares linear regression (Figure 2b). The obtained equation, $\log(V) = \log(n) - 11.5$, can be further converted to $V = 10^{-11.5} \times n$, indicating that, within the limits of experimental error, the initial rate V is linearly related to the DW coverage n when $n \leq 20$.

However, when the DW coverage further increases from 20 to 60 per AuNP, decreased reaction rates were observed (Figure 2c and Figure S2). We suspect that DW probes may interfere with each other through charge repulsion and steric hindrance when overlapping at the same track region. To test this hypothesis, initial rates of a nanomachine with a shorter DW (l = 42 nt) were measured and plotted against DW coverages. Because a shorter DW will cover a smaller track space, a higher DW coverage can be used before the overlapping occurs. In other words, the critical value of n, n_{crit}, that is, the coverage that enables the maximum initial rate, will shift to a higher value. Indeed, when DW lengths were

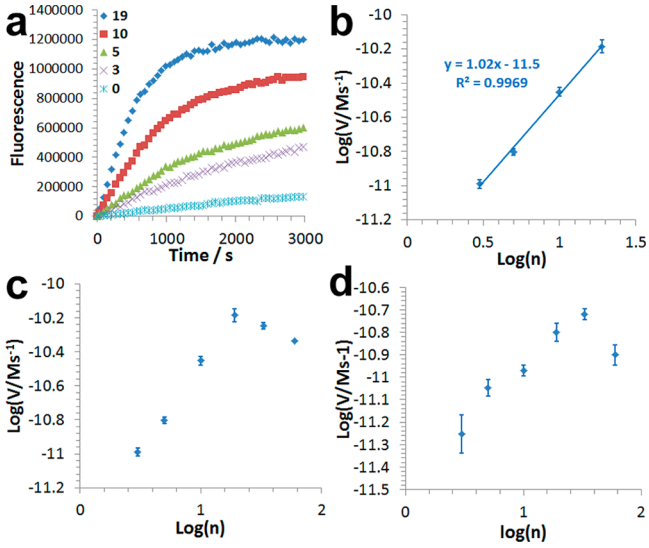

Figure 2. Effect of the DW design (coverage n and length l) on the kinetics of 3-D DNA nanomachine, DW–SR–AuNP. Each reaction mixture contained 20 U nicking endonuclease and 100 pM DW–SR–AuNPs that are of different DW densities or lengths. The SR coverage m was maximized and measured to be ~350 per AuNP for this set of experiment. (a) Fluorescence increases as a function of time from DW–SR–AuNP, with DW densities n varying from 0 to 19 per AuNP. (b) Quantitative relationship between n and corresponding initial rates V of DW–SR–AuNP, where n is between 0 and 19 and l = 57 nt. (c) Quantitative relationship between n and V, where n is between 0 and 60 and l = 57 nt. (d) Quantitative relationship between n and V, where n is between 0 and 60 and l = 42 nt. Error bars represent one standard deviation from triplicate analyses.

reduced from 57 to 42 nt, n_{crit} shifted from 20 to 40 per AuNP (Figure 2d), confirming the critical roles of DW length and coverage on the performances of the 3-D DNA nanomachine.

Because of the dual roles of SR as both cleavable substrate on the track and the payload-containing unit, SR coverage is another key factor that can potentially affect the kinetics of the DNA nanomachine. To understand the effect of SR, we fixed the coverage of the DW to be 20 per AuNP (l = 57 nt) and altered the SR coverage m from 0 to ~350 per AuNP. As shown in Figure 3a, DNA nanomachines of higher SR coverage release more fluorescent payloads. However, increases in SR coverage do not necessarily lead to a faster initial rate, as shown in Figure 3b. When we plotted the measured initial rate V *versus* SR coverage m in their logarithmic forms, the data fit a straight line when m is between m = 10 and m = 163, with a slope of ~0.5 (Figure 3c). Increasing m from 163 (about half of the maximum value) to the maximum value does not influence the initial rate (Figure 3d), so we determined a quantitative relationship between V and m as $V \approx 10^{-11.3} m^{1/2}$ ($m \leq 1/2\ m_{max}$).

In addition to DW and SR, we have also studied the effects of concentrations of nicking endonuclease (Figure S3) and nanomachines in a solution (Figure S4). As shown in Figure S3C, the initial rate V of the nanomachine is linearly dependent on the concentration of the nicking endonuclease [E] when [E] ≤ 5 U/100 μL. When [E] > 5 U/100 μL, no further increase in the initial rate was observed (Figure S3D). As shown in Figure S4, V is also linearly dependent on the concentration of the nanomachine [AuNP] throughout the range tested (6.25 to 200 pM). We also studied the effect of nanoparticle size on the performance of the 3-D nanomachine. As shown in Figure S5, a

DOI: 10.1021/acsnano.5b07102
ACS Nano 2016, 10, 2324–2330

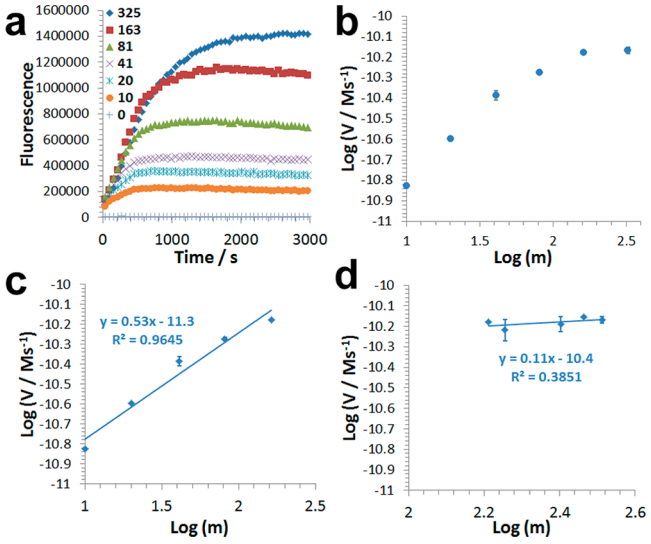

Figure 3. Effect of the SR coverage on the kinetics of the 3-D DNA nanomachine. Each reaction mixture contained 20 U nicking endonuclease and 100 pM DW−SR−AuNP that are of different SR densities. For each DW−SR−AuNP in this set of experiments, DW length *l* was fixed at 57 nt and DW coverage *n* was fixed at ~20 per AuNP. (a) Fluorescence increase as a function of time from DW−SR−AuNP with SR densities *m* varying from 0 to 325 per AuNP. (b) Quantitative relationship between *m* and corresponding initial rates *V*, where *m* is between 0 and 325. (c) Quantitative relationship between *m* and *V*, where *m* is between 0 and 163. (d) Quantitative relationship between *m* and *V*, where *m* is between 163 and 325. Error bars represent one standard deviation from triplicate analyses.

higher end-point fluorescence signal was observed when 40 nm AuNP was used to construct the nanomachine because of a higher SR coverage of a 40 nm DW−SR−AuNP (~500 per AuNP) than that of a 20 nm one (~350 per AuNP). However, a faster initial rate was observed for the nanomachine that was constructed using a 20 nm AuNP. We suspected that this result is due to a higher SR density on a 20 nm AuNP as a result of a stronger curvature effect.[29] To test this assumption, we converted the coverage of SR on a 20 nm AuNP into its actual density, which was determined to be $6.79 \times 10^{12}/\text{cm}^2$. The density for SR on a 40 nm AuNP was calculated to be $2.49 \times 10^{12}/\text{cm}^2$, which is significantly lower than half of the SR density on the 20 nm AuNP and thus resulted in a lower initial rate. This result further confirmed the importance of making use of nanoparticles and their curvature effects in designing the 3-D DNA nanomachines to ensure sufficient payload density and rapid release.

We further derived an empirical equation for the overall initial rate to be $V = K\cdot[\text{E}]\cdot[\text{AuNP}]\cdot m^{1/2}\cdot n$, where K is a constant, $[\text{E}] \leq 5$ U/100 μL, $m \leq 1/2\ m_{max}$, and $n \leq n_{crit}$. This equation suggests that, in order to maximize the efficiency for payload release, the coverage of the substrate on a 3-D DNA nanomachine should be maximized, as well as the amount of enzymes, to their critical values ($m > 1/2\ m_{max}$, $[\text{E}] > 5$ U/100 μL). When the values of these two parameters are above their critical values, the empirical equation can be modified to $V = K'\cdot[\text{AuNP}]\cdot n$ ($n \leq n_{crit}$), revealing the critical roles of DW design (both coverage and length) on the efficiency of payload release.

As the product of [AuNP] and n is the total concentration of DW in the solution, the equation, $V = K'\cdot[\text{AuNP}]\cdot n$ ($n \leq n_{crit}$), can be further simplified to $V = K'\cdot[\text{DW}]$ ($n \leq n_{crit}$). This linear relationship suggests that it is possible to quantify the amount of active DW as a "target" in a solution by measuring the initial rate of the nanomachine.[30] On the basis of this principle, we further tailored our 3-D nanomachine into a practically useful nanosensor for amplified detection of target nucleic acids.

Engineering the 3-D DNA Nanomachine into a DNA Nanosensor. To convert a 3-D DNA nanomachine into a nanosensor, it is critical to be able to switch on/off the DNA nanomachine in a target-specific manner. To achieve this goal, we introduce a protecting DNA probe P that can deactivate the nanomachine by caging DW through hybridization. As shown in Figure 4a, P contains a long complementary region to the DW (green and red), including a short DNA sequence (red

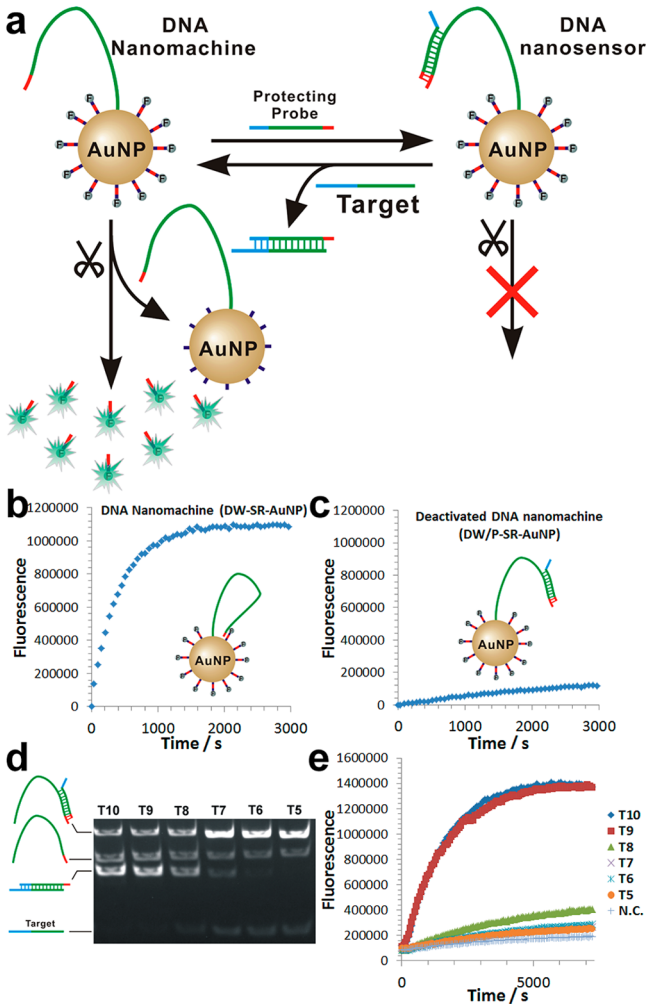

Figure 4. (a) Schematic illustrating the strategy to convert a 3-D DNA nanomachine into a DNA nanosensor by introducing a protecting DNA design and a toehold exchange mechanism. (b) Fluorescence increase as a function of time from a 100 pM active DNA nanomachine. (c) Fluorescence increase as a function of time when the DNA nanomachine is deactivated by hybridizing DW with the protecting DNA probe (P). (d) Native PAGE characterization of toehold exchange probe designs in solution. Each lane contains 2 μM DW/P duplex and 1 μM target DNA. The toehold length on P varies from 10 (lane 1) to 5 (lane 6). (e) Fluorescence increase as a function of time from a mixture containing 100 pM DNA nanosensors bearing different toehold lengths and 20 nM target DNA.

DOI: 10.1021/acsnano.5b07102
ACS Nano 2016, 10, 2324−2330

region) that can partially block the nicking recognition site. P also contains a short DNA overhang (the blue region), which serves as a DNA toehold. In the presence of a target nucleic acid, the target can release P from the DW through a toehold exchange mechnism.[31,32] Once P is released, the ability of the DNA nanomachine to generate fluorescent signals is restored. As the active DW in the system corresponds to the amount of target that is used to release P, a quantitative relationship can then be established between initial rates of the nanomachine and concentrations of the input target.

To demonstrate proof-of-principle, we chose a sequence from a drug (rifampin)-resistant strain of *Mycobacterium tuberculosis* (MTB) as a model target. We then incorporated the target-specific sequence into the DW and P. The performance of the MTB-specific 3-D DNA nanomachine is shown in Figure 4b. The initial rate was measured to be $V = 7.39 \times 10^{-11}$ M s^{-1}. The introduction of P was found to effectively deactivate the nanomachine to almost background level ($V = 2.46 \times 10^{-12}$ M s^{-1}, Figure 4c). By further investigating the deactivation mechanism, as shown in Figure S6, we realized that in addition to partially blocking the nicking recognition site on DW, increases in rigidity and steric hindrance of DW upon hybridizing to P also play a significant role in this high deactivation efficiency.

The use of the toehold exchange mechanism is a key to expand our sensor to any target sequence of interest because it does not require the target to contain any nicking recognition sequences. To ensure sufficient deactivation of the nanomachine, we fixed the enzyme-blocking region to be 5 nt long and varied the toehold length from 5 to 10 nt. Previously, Yin and co-workers have demonstrated that a toehold length of 7 is sufficient to displace a DNA strand with a 5 nt reverse toehold on the same DNA template for most toehold exchange reactions.[32] We found a similar result when characterizing our toehold exchange probes in a homogeneous solution using gel electrophoresis (Figure 4d). However, when DW/P duplexes were conjugated onto a AuNP, a minimum toehold length of 9 nt was required to trigger a sufficient strand exchange reaction and restore the activity of the nanomachine (Figure 4e), likely due to strong charge repulsion from the dense DNA layer on each AuNP.

Nucleic Acid Analysis Using the DNA Nanosensor. Upon construction of the DNA nanosensor on the basis of the 3-D DNA nanomachine, we then characterized its analytical performance for quantifying the target DNA. In a typical experiment, we first incubated the sensor with the target to regenerate the nanomachine through toehold exchange reactions. As shown in Figure S7, this reaction is very efficient, requiring only 10 min to restore the activity of the nanomachine. The initial rates of the nanomachines were then measured by monitoring the fluorescence increase every 1 min for 5 min after the nicking endonuclease was added to power the nanomachine (Figure 5a). By plotting the initial rate against target concentration, we were able to detect target DNA across 3 orders of magnitude (5 pM to 5 nM) within 20 min (Figure 5b). Compared to other isothermal DNA amplification techniques, such as rolling circle amplification and strand displacement assays, which typically take 1−2 h for amplification, our assay is faster.[33] The underlining mechanism for this fast signal response is due to our unique design, where all DNA probes are co-conjugated on the same AuNP, thus greatly enhancing their local effective concentrations during the enzymatic reaction.

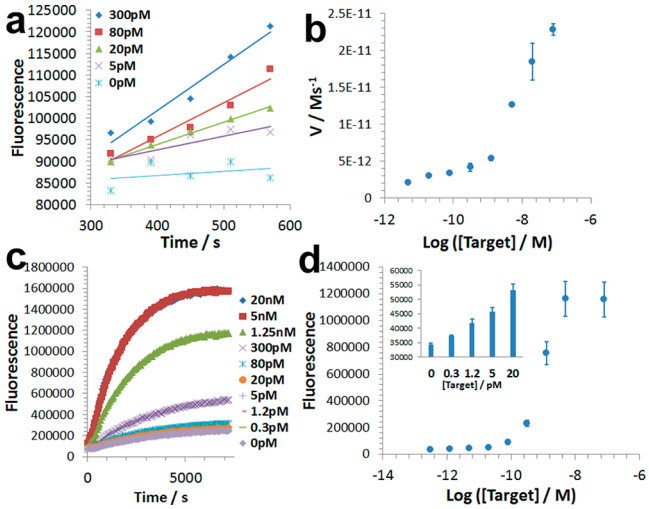

Figure 5. Quantification of DNA targets using DNA nanosensors. (a) Determining the initial rate of DNA nanosensors in the presence of targets at varying concentrations. (b) Initial rate of DNA nanosensors as a function of target concentration varying from 5 pM to 80 nM. (c) Real-time monitoring of fluorescence increase of DNA nanosensors in the presence of targets over a period of 2 h. (d) Quantification of targets using end-point fluorescence measured at 1 h. Error bars represent one standard deviation from triplicate analyses.

The sensor is also very specific, evidenced by the background level nanomachine activities when incubating with a scrambled DNA control and a control containing 0.1 mg/mL salmon sperm genome DNA fragments (Figure S8). By further tuning the lengths of the reverse toehold on DW/P duplex from 5 to 10 nt while fixing the forward toehold length to be 9 nt, we were able to differentiate the target DNA from a control sequence that is identical to the target except for bearing a single point mutation (Figure S9).

In addition to using the initial rate to detect target DNA, it is also possible to make use of the final fluorescence increase from the sensor to quantify targets (Figure 5c). As shown in Figure 5d, by running 100 pM nanomachine sensors with the target at varying concentrations at 37 °C for 1 h, we were able to push the detection limit to 300 fM. This detection limit could be further improved to 75 fM by using sensors of a lower concentration (50 pM) to minimize the background fluorescence (Figure S10). A longer reaction time (*e.g.*, 2 h) was also required to achieve a better detection limit. Because a major source of background interference comes from the target-independent release of SR from the AuNP due to the residue DTT associated with the nicking enzyme, it is possible to further improve the assay performance by designing SR probes that are insensitive to DTT release, such as incorporating an internal quencher to the SR.

We also challenged our sensor for detecting target nucleic acids in a complicated sample matrix by spiking targets of varying concentrations into human serum samples that have been pretreated with proteinase K. As shown in Figure S11, the sensors are functional in 10-fold-diluted human serum samples, and a detection limit of 20 pM was achieved. However, it is very challenging to directly quantify target nucleic acids from undiluted serum samples due to the high background signal. To address this challenge, we integrated a 20 min commercially available serum DNA extraction step into our assay. This step eliminated all matrix effects and allowed us to detect a target as

DOI: 10.1021/acsnano.5b07102
ACS Nano 2016, 10, 2324−2330

low as 20 pM directly from undiluted human serum samples (Figure S12).

CONCLUSIONS

Unlike most DNA nanomachines that are one- or two-dimensional, our enzyme-powered DNA nanomachine is constructed on a three-dimensional DNA–AuNP track. The co-conjugation of all DNA components on a single AuNP ensures a well-defined space for DNA walking. The corresponding increases in local effective concentrations of DNA probes also accelerated enzymatic cleavage, making the 3-D DNA nanomachine amenable for the task of rapid payload release. The concept of integrating multiple functional components on a single nanoparticle has also made it easier to expand the functionality of the nanomachine. For example, we have successfully tailored it into a highly sensitive and rapid nanosensor for specific nucleic acid target by incorporating a toehold exchange mechanism. Our success in designing the 3-D DNA nanomachine and subsequent nanosensor opens up new concepts and strategies in dynamic DNA nanotechnology, which may lead to the development of novel DNA nanodevices, drug delivery vehicles, and biosensors.

METHODS

Materials and Reagents. Solutions of gold nanoparticles (AuNPs) (20 nm in diameter), magnesium chloride hexahydrate ($MgCl_2 \cdot 6H_2O$), Tween 20, dithiothreitol (DTT), salmon sperm DNA fragments, 10× phosphate-buffered saline (PBS) solution, and human serum (product number H6914) were purchased from Sigma (Oakville, ON, Canada). Ammonium persulfate (APS), *N,N,N′,N′*-tetramethylethylenediamine (TEMED), 40% acrylamide/bis solution, DNA loading buffer, and 20 bp molecular ruler were purchased from Bio-Rad Laboratories, Inc. (ON, Canada). Nicking endonuclease (Nb.BvCI) and CutSmart buffer (NEBuffer) were purchased from New England Biolabs (Canada). Proteinase K and a plasma/serum circulating DNA purification kit were purchased from Norgen Biotek Corp. (Thorold, ON, Canada). NANOpure H_2O (>18.0 MΩ), purified using an Ultrapure Milli-Q water system, was used for all experiments. All DNA samples were purchased from Integrated DNA Technologies (Coralville, IA) and purified by high-performance liquid chromatography. The DNA sequences and modifications are listed in Table S1.

Preparation and Characterization of the 3-D DNA Nanomachine. Preparation of the 3-D DNA nanomachine was achieved by co-conjugating functional DNA probes onto gold nanoparticles according our previously established method.[34] In a typical experiment, the thiolated DW and SR oligonucleotides were mixed at a ratio of 1 to 20. A 20 μL solution of this mixture containing 2.5 μM DW oligonucleotides and 50 μM SR oligonucleotides was mixed with 1 mL of 1 nM AuNPs. This mixture was incubated at room temperature for 12 h and then was slowly mixed with 20 μL of 3 M NaCl, followed by 10 s of sonication. This process of addition of NaCl and sonication was repeated five times with a 1 h interval to maximize the oligonucleotide loading amounts.[35] The solution was then incubated at room temperature for 24 h. After incubation, the solution was centrifuged at 13 500 rpm for 30 min to separate the DNA-functionalized AuNPs (DNA–AuNPs) from the unreacted reagents. The DNA–AuNPs were washed three times with 1× PBS buffer (pH 7.4) containing 0.01% Tween 20 and finally redispersed in PBS buffer.

After preparation, UV–vis spectrometry was used to characterize the quality of each DNA–AuNP solution and determine the concentration of the DNA–AuNP. Specifically, a maximum absorbance value of each DNA–AuNP solution was measured and compared to that of the unconjugated AuNP, whose concentration was provided by the vendor (1.16 nM). The wavelength at which the maximum AuNP absorbance could be observed typically underwent a red shift of 4–6 nm upon the conjugation of DNA oligonucleotides. The coverage of SR oligonucleotides on each AuNP was then determined by releasing SR from AuNP using 20 mM DTT and measuring fluorescence of the FAM dye that was labeled on SR.[36] Fluorescence was measured using a multimode microplate reader (SpectraMax i3, Molecular Devices), and SR coverage was quantified by using FAM-labeled SR oligos as external standards. The coverage of DW on each AuNP was then estimated according to the SR coverage and the initial ratio between DW and SR.

For a typical nanomachine operation, a reaction mixture containing 100 pM DNA nanomachines, 20 U nicking endonucleases, and 1× NEB CutSmart buffer was incubated at 37 °C in a 96-well microplate. Fluorescence signals were measured immediately after adding the enzyme. This measurement was carried out every 1 min from the microplate using a multimode microplate reader with excitation/emission wavelength of 485/535 nm to monitor the released FAM-labeled SR.

Preparation and Characterization of the DNA Nanosensor. The procedure for preparing and characterizing the DNA nanosensor is the same as that for the DNA nanomachine, except that 2.5 μM DW was first hybridized with equal amounts of the protecting DNA P through an annealing process. The optimal P design is first characterized using native PAGE gel electrophoresis. Briefly, a reaction mixture containing 1 μM annealed DW/P duplex of varying toehold lengths, 1 μM free DW, and 1 μM target MTB DNA was incubated at 37 °C for 30 min. Reaction mixtures were then loaded onto 12% PAGE gel, and a voltage of 110 V was applied. After electrophoresis, the gel was stained with ethidium bromide and imaged using a Gel Doc XR+ imager system (BioRad).

Detection of a MTB DNA Target Using the DNA Nanosensor. For a typical reaction, reaction mixtures containing 100 pM DNA nanosensors and varying concentrations of target DNA (either in buffer or spiked in 10-fold diluted human serum samples) were incubated at 37 °C for 10 min. To each mixture was added 20 U nicking endonuclease. Immediately after the enzyme was added, fluorescence signals were measured every 1 min from the microplate containing the reaction mixture using a multimode microplate reader with an excitation/emission wavelength of 485/535 nm.

To quantify target DNA from undiluted human serum samples, targets of varying concentrations were first spiked into undiluted human serum samples. To mimic the process for analyzing circulating nucleic acids, human serum samples were pretreated using proteinase K to release bound nucleic acids from proteins. A commercial plasma/serum circulating DNA purification kit (Norgen BioTek, Thorold, Canada) was then used to isolate and preconcentrate all DNA components from human serum samples according to the manufacturer's instructions. The concentrated samples were then diluted using 1× NEB CutSmart buffer and quantified using DNA nanosensors as described above.

ASSOCIATED CONTENT

Supporting Information

The Supporting Information is available free of charge on the ACS Publications website at DOI: 10.1021/acsnano.5b07102.

Table S1 and Figures S1–S12 (PDF)

AUTHOR INFORMATION

Corresponding Author

*E-mail: fli@brocku.ca.

Notes

The authors declare no competing financial interest.

ACKNOWLEDGMENTS

We thank the Natural Sciences and Engineering Research Council of Canada and the Brock University Start-Up Fund for financial support. We thank Dr. Heather Gordon for her insightful suggestions to this work and the revision to this manuscript.

DOI: 10.1021/acsnano.5b07102
ACS Nano 2016, 10, 2324–2330

REFERENCES

(1) Abendroth, J. M.; Bushuyev, O. S.; Weiss, P. S.; Barrett, C. J. Controlling Motion at the Nanoscale: Rise of the Molecular Machines. *ACS Nano* **2015**, *9*, 7746−7768.

(2) Bath, J.; Turberfield, A. J. DNA Nanomachines. *Nat. Nanotechnol.* **2007**, *2*, 275−284.

(3) Zhang, D. Y.; Seelig, G. Dynamic DNA Nanotechnology Using Strand-Displacement Reactions. *Nat. Chem.* **2011**, *3*, 103−113.

(4) von Delius, M.; Leigh, D. A. Walking Molecules. *Chem. Soc. Rev.* **2011**, *40*, 3656−3676.

(5) Pan, J.; Li, F.; Cha, T.-G.; Chen, H.; Choi, J. H. Recent Progress on DNA Based Walkers. *Curr. Opin. Biotechnol.* **2015**, *34*, 56−64.

(6) Sherman, W. B.; Seeman, N. C. A Precisely Controlled DNA Biped Walking Device. *Nano Lett.* **2004**, *4*, 1203−1207.

(7) Shin, J.-S.; Pierce, N. A. A Synthetic DNA Walker for Molecular Transport. *J. Am. Chem. Soc.* **2004**, *126*, 10834−10835.

(8) Omabegho, T.; Sha, R.; Seeman, N. C. A Bipedal DNA Brownian Motor with Coordinated Legs. *Science* **2009**, *324*, 67−71.

(9) Yin, P.; Yan, H.; Daniell, X. G.; Turberfield, A. J.; Reif, J. H. A Unidirectional DNA Walker That Moves Autonomously Along a Track. *Angew. Chem., Int. Ed.* **2004**, *43*, 4906−4911.

(10) Bath, J.; Green, S. J.; Turberfield, A. J. A Free-Running DNA Motor Powered by a Nicking Enzyme. *Angew. Chem., Int. Ed.* **2005**, *44*, 4358−4361.

(11) Cha, T.-G.; Pan, J.; Chen, H.; Salgado, J.; Li, X.; Mao, C.; Choi, J. H. A Synthetic DNA Motor That Transports Nanoparticles Along Carbon Nanotubes. *Nat. Nanotechnol.* **2013**, *9*, 39−43.

(12) You, M.; Chen, Y.; Zhang, X.; Liu, H.; Wang, R.; Wang, K.; Williams, K. R.; Tan, W. An Autonomous and Controllable Light-Driven DNA Walking Device. *Angew. Chem., Int. Ed.* **2012**, *51*, 2457−2460.

(13) Yang, Y.; Goetzfried, M. A.; Hidaka, K.; You, M.; Tan, W.; Sugiyama, H.; Endo, M. Direct Visualization of Walking Motions of Photocontrolled Nanomachine on the DNA Nanostructure. *Nano Lett.* **2015**, *15*, 6672−6676.

(14) Wickham, S. F. J.; Endo, M.; Katsuda, Y.; Hidaka, K.; Bath, J.; Sugiyama, H.; Turberfield, A. J. Direct Observation of Stepwise Movement of a Synthetic Molecular Transporter. *Nat. Nanotechnol.* **2011**, *6*, 166−169.

(15) Wickham, S. F. J.; Bath, J.; Katsuda, Y.; Endo, M.; Hidaka, K.; Sugiyama, H.; Turberfield, A. J. A DNA-Based Molecular Motor That Can Navigate a Network of Tracks. *Nat. Nanotechnol.* **2012**, *7*, 169−173.

(16) Zhou, C.; Duan, X.; Liu, N. A Plasmonic Nanorod That Walks on DNA Origami. *Nat. Commun.* **2015**, *6*, 8102.

(17) Tian, Y.; Mao, C. Molecular Gears: a Pair of DNA Circles Continuously Rolls against Each Other. *J. Am. Chem. Soc.* **2004**, *126*, 11410−11411.

(18) Pei, R.; Taylor, S. K.; Stefanovic, D.; Rudchenko, S.; Mitchell, T. E.; Stojanovic, M. N. Behavior of Polycatalytic Assemblies in a Substrate-Displaying Matrix. *J. Am. Chem. Soc.* **2006**, *128*, 12693−12699.

(19) Lund, K.; Manzo, A. J.; Dabby, N.; Michelotti, N.; Johnson-Buck, A.; Nangreave, J.; Taylor, S.; Pei, R.; Stojanovic, M. N.; Walter, N. G.; Winfree, E.; Yan, H. Molecular Robots Guided by Prescriptive Landscapes. *Nature* **2010**, *465*, 206−209.

(20) Zhang, H.; Lai, M.; Zuehlke, A.; Peng, H.; Li, X.-F.; Le, X. C. Binding-Induced DNA Nanomachines Triggered by Proteins and Nucleic Acids. *Angew. Chem., Int. Ed.* **2015**, *54*, 14326−14330.

(21) Jung, C.; Allen, P. B.; Ellington, A. D. A Stochastic DNA Walker That Traverses a Microparticle Surface. *Nat. Nanotechnol.* **2015**, DOI: 10.1038/nnano.2015.246.

(22) Li, F.; Zhang, H.; Lai, C.; Li, X.-F.; Le, X. C. A Molecular Translator That Acts by Binding-Induced DNA Strand Displacement for a Homogeneous Protein Assay. *Angew. Chem., Int. Ed.* **2012**, *51*, 9317−9320.

(23) Li, F.; Zhang, H.; Wang, Z.; Li, X.-F.; Le, X. C. Dynamic DNA Assemblies Mediated by Binding-Induced DNA Strand Displacement. *J. Am. Chem. Soc.* **2013**, *135*, 2443−2446.

(24) Li, F.; Lin, Y.; Le, X. C. Binding-Induced Formation of DNA Three-Way Junctions and Its Application in Real-Time Protein Detection and DNA Strand Displacement. *Anal. Chem.* **2013**, *85*, 10835−10841.

(25) Tang, Y.; Wang, Z.; Yang, X.; Chen, J.; Liu, L.; Zhao, W.; Le, X. C.; Li, F. Constructing Real-Time, Wash-Free, and Reiterative Sensors for Cell Surface Proteins Using Binding-Induced Dynamic DNA Assembly. *Chem. Sci.* **2015**, *6*, 5729−5733.

(26) Hinsch, B.; Kula, M. R. Physical and Kinetic Properties of the Site Specific Endonuclease Bam HI from Bacillus Amylolique-Faciens. *Nucleic Acids Res.* **1980**, *8*, 623−633.

(27) Pingoud, A.; Jeltsch, A. Recognition and Cleavage of DNA by Type-II Restriction Endonuclease. *Eur. J. Biochem.* **1997**, *246*, 1−22.

(28) Li, S.; Chen, N.; Zhang, Z.; Wang, Y. Endonuclease-Responsive Aptamer-Functionalized Hydrogel Coating for Sequential Catch and Release of Cancer Cells. *Biomaterials* **2013**, *34*, 460−469.

(29) Hill, H. D.; Millstone, J. E.; Banholzer, M. J.; Mirkin, C. A. The Role Radius of Curvature Plays in Thiolated Oligonucleotide Loading on Gold Nanoparticles. *ACS Nano* **2009**, *3*, 418−424.

(30) Li, J. J.; Chu, Y.; Lee, B. Y.-H.; Xie, X. S. Enzymatic Signal Amplification of Molecular Beacons for Sensitive DNA Detection. *Nucleic Acids Res.* **2008**, *36*, e36.

(31) Zhang, D. Y.; Winfree, E. Control of DNA Strand Displacement Kinetics Using Tehold Exchange. *J. Am. Chem. Soc.* **2009**, *131*, 17303−17314.

(32) Zhang, D. Y.; Chen, S. X.; Yin, P. Optimizing the Specificity of Nucleic Acid Hybridization. *Nat. Chem.* **2012**, *4*, 208−214.

(33) Zhang, H.; Li, F.; Dever, B.; Li, X.-F.; Le, X. C. DNA-Mediated Homogeneous Binding Assays for Nucleic Acids and Proteins. *Chem. Rev.* **2013**, *113*, 2812−2841.

(34) Li, F.; Zhang, H.; Dever, B.; Li, X.-F.; Le, X. C. Thermal Stability of DNA Functionalized Gold Nanoparticles. *Bioconjugate Chem.* **2013**, *24*, 1790−1797.

(35) Hurst, S. J.; Lytton-Jean, A. K.; Mirkin, C. A. Maximizing DNA Loading on a Range of Gold Nanoparticle Sizes. *Anal. Chem.* **2006**, *78*, 8313−8318.

(36) Demers, L. M.; Mirkin, C. A.; Mucic, R. C.; Reynolds, R. A.; Letsinger, R. L.; Elghanian, R.; Viswanadham, G. A Fluorescence-Based Method for Determining the Surface Coverage and Hybridization Efficiency of Thiol-Capped Oligonucleotides Bound to Gold Thin Films and Nanoparticles. *Anal. Chem.* **2000**, *72*, 5535−5541.

DOI: 10.1021/acsnano.5b07102
ACS Nano 2016, 10, 2324−2330